

Engineered pre-dentin with well-aligned hierarchical mineralized collagen fibril bundles promote bio-root regeneration

Journal of Tissue Engineering
Volume 15: 1–17
© The Author(s) 2024
Article reuse guidelines:
sagepub.com/journals-permissions
DOI: 10.1177/20417314241280961
journals.sagepub.com/home/tej



Lei Hu^{1*}, Dongmei Cheng^{1*}, Xin Yuan¹, Zhenhua Gao¹, Qiao Yi¹, Bin Zhao¹, Fulan Wei², Junji Xu¹, Zhipeng Fan¹, Yi Liu¹, Xiumei Wang³, Fuzhai Cui³, Chunmei Zhang¹, Jinsong Wang^{1,4} and Songlin Wang^{1,4}

Abstract

Stem cell-mediated bio-root regeneration is an alternative tooth replacement strategy; however, physiologically functional bio-root regeneration with distinctive dentin structure remains challenging. In this study, the distinct arrangements of collagen fibril bundles were identified that account for hierarchical structural differences between dentin, cementum, and alveolar bone. Thus, an “engineered pre-dentin” was fabricated, which was a dentin hierarchical structure mimicking collagen (MC) scaffold, with well-aligned hierarchical mineralized collagen fibril bundles. The results revealed that it has a stronger effect on promoting biological root regeneration in nude mice and miniature pigs with dental pulp stem cell (DPSC) and periodontal ligament stem cell (PDLSC) sheets compared to hydroxyapatite tricalcium phosphate (HA/TCP). The success rate in the MC group was also higher than that in the HA/TCP group (67% and 33%, respectively). In conclusion, the hierarchical dentin-mimicking scaffold can enhance the regeneration of bio-roots, which provides a promising strategy for tooth regeneration.

Keywords

Bio-root, dentin mimicked scaffold, hierarchical structure, tissue regeneration

Date received: 2 May 2024; accepted: 21 August 2024

Introduction

With advances in dental stem cell biotechnology and cell-based tooth regeneration, the regeneration of living teeth is an ideal strategy for tooth loss rehabilitation.^{1,2} Our previous studies showed that functional bio-roots with periodontal ligament/dentin-cementum structures can be

regenerated using dental pulp stem cell (DPSC)/periodontal ligament stem cell (PDLSC) sheets and hydroxyapatite/tricalcium phosphate (HA/TCP) scaffolds in miniature pigs.³ The engineered bio-roots exhibited a structure similar to natural roots, was sufficiently robust to support an artificial crown, and performed well. Our subsequent study showed that using allogeneic DPSC/PDLSC sheets

¹Beijing Key Laboratory of Tooth Regeneration and Function Reconstruction, Beijing Laboratory of Oral Health and School of Stomatology, Capital Medical University, Beijing, China

²Department of Orthodontics, Shandong Provincial Key Laboratory of Oral Biomedicine, School of Stomatology, Shandong University, Jinan, China

³State Key Laboratory of New Ceramics and Fine Processing, School of Materials Science and Engineering, Tsinghua University, Beijing, China

⁴Department of Biochemistry and Molecular Biology, Capital Medical University School of Basic Medical Sciences, Beijing, China

*The authors contributed equally to this work.

Corresponding authors:

Songlin Wang, Beijing Key Laboratory of Tooth Regeneration and Function Reconstruction, Beijing Laboratory of Oral Health and School of Stomatology, Capital Medical University, You An Men Wai, Beijing 100069, China.

Email: slwang@ccmu.edu.cn

Lei Hu, Beijing Key Laboratory of Tooth Regeneration and Function Reconstruction, Beijing Laboratory of Oral Health and School of Stomatology, Capital Medical University, Tian Tan Xi Li No. 4, Beijing 100050, China.

Email: hulei@ccmu.edu.cn



as a cell transplantation source in a miniature pig model can also mediate functional bio-root regeneration without eliciting immune rejection.⁴ Compared to dental implants, the structure, biomechanical properties, and elemental composition of bio-roots are similar to those of natural teeth, indicating that it is a promising strategy for tooth loss rehabilitation.⁵ However, the bio-root lacks dentin microstructure. Thus, regenerating a physiologically structured and functional bio-root remains challenging.

Dentin, the main component of tooth roots, is a hierarchically organized and mineralized tissue. The mineral component in dentin consists primarily of hydroxyapatite (HA), while the organic portion contains mainly collagen, non-collagenous proteins, and proteoglycans.⁶ Similar to the formation of bone, the generation of dentin is the result of biomineralization, which is a precise hierarchical self-assembly process from the microscopic to the macroscopic scale, during which organic molecules regulate and control the deposition of inorganic minerals.⁷ Based on the structure of the mineralized tissue, a hierarchical scaffold that mimics the biomineralization process has demonstrated an increased potential of tissue regeneration.^{8–11} Although the inorganic matter contents of dentin and bone are similar, dentin shows relatively higher mineralization than bone and has different macroscopic structures and properties. Therefore, mimicking the dentin-specific self-assembly process is critical for tooth root regeneration.

In this study, the hierarchical structures of tooth root tissues were analyzed using various microscopic approaches at different levels, including nanometer, micrometer, millimeter, and macroscopic levels. The primary mechanisms that underlie the structural differences amongst the root tissues have been investigated. Then, a dentin-mimicking collagen (MC) scaffold, “engineered pre-dentin,” was fabricated by elaborately assembling collagen based on the specific arrangement of collagen fibril bundles in dentin. We investigated the function of the MC scaffold during DPSCs odontogenic differentiation and its bio-root regenerative potential *in vivo*, which have demonstrated that the MC scaffold could be a promising tool for tooth root regeneration.

Materials and methods

Miniature pigs, mice

The animal study was approved by the Animal Care and Use Committee of Capital Medical University (Ethical code: AEEI-2015-080). Miniature pigs (aged 18 months, weighing 50–60 kg) were acquired from the Animal Science Institute of Chinese Agriculture University. BALB/c nude mice were purchased from Beijing Vital River Laboratory Animal (Beijing, China). This study complied with ARRIVE (Animal Research: Reporting of In Vivo Experiments) guidelines for preclinical animal

studies. Miniature pigs were fed under clean conditions, anesthetized by injecting ketamine chloride (6 mg/kg) and xylazine (0.6 mg/kg) intravenously before surgery. Loss of more than 20% of body weight and/or development of severe systemic diseases were the endpoint of experiment and the criteria for euthanasia. Mice were maintained in a specific pathogen-free animal facility and kept under conventional conditions with free access to water and food. At 1, 2, 4, and 8 weeks after transplantation, the mice were euthanized by carbon dioxide asphyxiation.

Samples

The dentin, cementum, and surrounding alveolar bone of third molars ($N=10$) was obtained from individuals aged 11 to 18 years in this study according to an approved protocol issued by the Capital Medical University School of Stomatology, Beijing, P. R. China (approval number: KJ-2019-006F-C-02-FS(CS)). After extraction, soft tissues around the tooth root were removed, then the samples were stored in Hank's Balanced Salt Solution (HBSS) at 4 °C, to avoid dehydration and loss of minerals. Slices were cut in two planes with an Metallographic low-speed precision cutting machine (METCUT-5, MetLab, USA) along their longitudinal axis, parallel to the buccal-lingual surfaces and along their horizontal axis, parallel to the mesio-distal surfaces. The thin specimens' slices were wet-polished using 800- to 6000-grit SiC polishing paper and were also briefly cleaned ultrasonically before treatment.

Scanning electron microscopy (SEM)

To prepare the sample for SEM, the specimens' slices were treated with the citric acid buffer (pH 3.8) for 10 min and then fixed with 2.5% glutaraldehyde for 24 h. Next, they were washed in double-distilled water three times and dehydrated in an ascending ethanol series (50%–100%). Then, the slices were dried with supercritical CO₂, coated with gold palladium to prevent charging, and observed with a GeminiSEM 500 (German) scanning electron microscope at 3 kV. Photomicrographs at different magnifications were obtained in order to achieve a representative view of each group.

Transmission electron microscope (TEM)

For TEM examinations of the specimens' slices, the samples were treated with 5% EDTA for 4 weeks, fixed with 2.5% glutaraldehyde overnight, washed with 0.1 M sodium dimethylarsenate buffer (pH 7.2) three times and then fixed again with 1% osmium buffer for 2 h, flashed with sodium dimethylarsenate buffer, and finally dehydrated with gradient alcohol (50%–100%). For observation, the specimens' slices were embedded in resin, and sliced into

70 nm sections with a grinding machine (METPOL-2V, MetLab, USA). Each slice was covered with a Formvar-coated, carbon-reinforced copper grid, and dyed with uranyl acetate and lead citrate for observation under a Leica (TP1020, Germany).

Focused ion beam scanning electron microscope (FIB-SEM)

For FIB-SEM tomography, the dentin, cementum and alveolar bone samples were demineralized in parallel with mild fixation, conditioned with alcian blue to stabilize non-collagenous organic components, and fixed with glutaraldehyde. The samples were high-pressure frozen and freeze-substituted, which preserves the dimensions and architecture as in the hydrated state. The samples were then embedded in Epon and 100 nm-thick specimens were prepared by FIB milling and the lift-out technique, using a Helios Nanolab 600 (FEI, Boston MA, USA), following an automated procedure (AutoTEM G2 software, FEI, Boston MA, USA) at 30 keV. Specimens were mounted on a semi-grid for thinning to obtain electron transparency (approximating a 100 nm section thickness) using current reduction from 0.46 nA to 28 pA, at 30 keV. Final polishing of the thinned samples was conducted at ion acceleration voltages of 16 keV and then 5 keV. The imaging was performed using a dual-beam FEI Helios 600 Nanolab FIB-SEM operating in the serial-surface view mode with the accelerating voltage of 2 kV, beam current of 0.34 nA, voxel size of 3.9 nm × 3.9 nm × 50 nm and dwell time of 10 μs. The resultant three-dimensional (3D) stacks were processed using Fiji and the labeling of individual collagen fibrils was carried out using the local threshold algorithm in Avizo 9.2 (FEI, Boston MA, USA).

RNA-SMART sequencing

The SMART-Seq[®] HT Kit and TruSeq[®] RNA Sample Preparation Kit (Illumina, USA) were employed to extract RNA from dentin, cementum and periodontal ligament of human teeth and to generate paired-end libraries. mRNAs bearing poly-A were purified using magnetic beads conjugated with poly-T, which was followed by reverse transcription. Following synthesis using DNA polymerase I and RNase H, the final cDNA library was prepared by PCR. The clusters were produced by the cBot and subsequently sequenced on the Illumina HiSeq Xten (Illumina, USA). Hisat2 (version 2.0.4) was deployed to map the purified reads to the human hg38 reference genome, allowing for two mismatches. Differential gene expression was analyzed by edgeR. The false discovery rate (FDR) was utilized to determine the significance threshold of p-values. Genes were considered differentially expressed if they met the following criteria: FDR < 0.05 and fold-change ≥ 2.

PCR array

In order to illustrate the expression levels of different collagen genes in dentin, cementum, and alveolar bone, we constructed a human PCR array analysis. The related collagen genes' expression profiles were analyzed according to the manufacturer's protocol (WcGene Biotech, Shanghai, China). Data were analyzed using WcGene Biotech software. Genes with fold-changes greater than 2.0 or less than 0.5 were considered to be statistically significant.

Quantitative real-time polymerase chain reaction (qRT-PCR)

Total mRNA was extracted by RNAprep pure Cell Kit (TIANGEN, Beijing, China) according to the manufacturer's instructions. The transcription of total RNA into cDNA was carried out with FastQuant RT Kit (TIANGEN, Beijing, China). Real-time polymerase chain reaction (PCR) reactions were carried out with the SuperReal PreMix Plus SYBR Green PCR kit (TIANGEN, Beijing, China). The primers used for the specific genes are shown in the Supplemental Table 1.

The culture of DPSCs and PDLSCs

Human impacted third molars were collected from five healthy male patients (16–20 years old) from Beijing Stomatological Hospital, Capital Medical University, and all treatments were performed per the approved guidelines. Informed consent was obtained from all patients. Teeth were first disinfected with 75% ethanol and then washed with phosphate-buffered saline. The pulp tissue was obtained from the crown and root, periodontal ligament was scraped from the middle part of tooth root. Subsequently, the tissues were digested in a solution containing 3 mg/mL collagenase type I (Worthington Biochemical Corp., Lakewood, NJ, USA) and 4 mg/mL dispase (Roche Diagnostics Corp., Indianapolis, IN, USA) for 1 h at 37°C. Single-cell suspensions were obtained by passing through a 70-μm strainer. The cells were grown in alpha-MEM (Invitrogen, Carlsbad, CA, USA), supplemented with 15% fetal bovine serum (FBS; Invitrogen, Carlsbad, CA, USA), 2 mmol/L glutamine, 100 U/mL penicillin, and 100 μg/mL streptomycin (Invitrogen, Carlsbad, CA, USA) in a humidified incubator under 5% CO₂ at 37°C. The culture medium was changed every 3 days. Cells at passages 3–5 were used in subsequent experiments.

Mineralized potential detection

To evaluate the mineralization differentiation potential, 2 × 10⁴ DPSCs (three or four passages) were seeded into MC and HA/TCP and cultured in six well plates (BD Biosciences, Franklin Lakes, NJ, USA). Sub-confluent cultures were incubated in the mineralization medium

(Invitrogen, Carlsbad, CA, USA) for 4 weeks. The medium was changed every 2 days. Then cells were fixed with 70% ethanol, and qRT-PCR was used to determine the potential of mineralization differentiation of DPSCs.

Stem cell sheet induction

To induce the stem cell sheets, PDLSCs at third passages were sub-cultured in 10 cm dishes with 2×10^5 cells/well, and cultured in complete medium containing 20 $\mu\text{g}/\text{mL}$ vitamin C.^{4,5} About 10 days later, the cells on the edge of the dishes wrapped, indicating that cell sheets had formed and could be detached.

Fabrication of the dentin MC scaffold or HA/TCP scaffold

The dentin MC scaffold was developed by key laboratory of advanced materials of ministry of education school of Materials Science and Engineering, Tsinghua University, by mimicking the collagen fibril bundles arrangement of natural dentin¹⁰, after compared several widely used materials (Supplemental Figure S1). Briefly, the concentration of type I collagen was prepared as a 5.0×10^{-5} – 5.0×10^{-3} g/mL H_3PO_4 solution, and $\text{Ca}(\text{OH})_2$ solution was added slowly so that the molar ratio was $\text{Ca}/\text{P} = 1/1$ – $2/1$. The pH of the mixed system was then adjusted by adding NaOH solution slowly to achieve a pH of 6–8. Following the appearance of the white precipitate, the solution was left to stand for 48 h and then centrifuged to concentrate the precipitate. This process yielded the mineralized collagen gelatin jelly, which was then filled into molds prepared in advance. The collagen scaffolds were then subjected to freeze-drying, resulting in the formation of collagen scaffolds. Subsequently, crosslinking was performed using glutaraldehyde in an ethanol solution, with concentrations ranging from 0.005 to 0.25 wt%. The chromatographic column was then washed with pure water and autoclaved, resulting in the formation of the MC scaffold. The HA/TCP scaffolds were constructed as described in our previous study.⁴

Construct of bio-root complex before implantation

The second or third passages of DPSCs were digested with 0.05% trypsin, centrifuged, and resuspended in 0.5 mL culture medium. About 2×10^6 DPSCs were seeded onto MC or HA/TCP scaffolds, as described in our previous study.^{4,5} Then, the vitamin C-induced integral PDLSCs sheet was used to wrap around the MC or HA/TCP to form MC or HA/TCP/DPSCs/PDLSCs sheet complex.

Transplantation in nude mice

MC or HA/TCP combined with DPSCs/PDLSCs sheet complex transplanted subcutaneously into the dorsal surfaces of

10-week-old BALB/c nude mice ($N=24$, in each mouse, left was MC group and right was HA/TCP group). HA/TCP group as control. These procedures were performed in accordance with an approved animal protocol. At 1, 2, 4, and 8 weeks, the transplants were harvested (each group has six samples at one timepoint), fixed with 10% formalin, decalcified with buffered 10% EDTA (pH=8.0), and then embedded in paraffin.

Immunofluorescence and immunohistochemistry

Paraffin-embedded tissue sections, with a 5- μm thickness, were deparaffinized using a series of xylene baths and rehydrated using graded alcohols and water. For fluorescent immunohistochemistry of DSPP, rabbit polyclonal anti-collagen I (Abcam, ab34710, 1:300, Cambridge, UK) and Alexa Fluor 488 goat anti-rabbit IgG (Life Technologies, 1:500, Carlsbad, CA, USA) were used, and then nuclei were stained with DAPI (Invitrogen, Carlsbad, CA, USA). For immunohistochemistry of DSPP expression, anti-DSPP (Santa Cruz, sc-398631, 1:200, Dallas, Texas, USA) and anti-mouse or anti-rabbit IgG κ binding protein-HRP (Santa Cruz, sc516102, sc2357, 1:500, Dallas, Texas, USA) were used, and a DAB kit was used to detect primary antibodies. HE stained images were captured using a Leica DM 4000 microscope (Leica, Germany), and immunofluorescent images were captured using a Leica TCS SP5 confocal microscope (Leica, Germany). The expression intensity was measured using the Image-Pro Plus 6.0 program (Media Cybernetics, Rockville, MD, USA).

Implantation of bio-root in miniature pig

Vitamin C-induced PDLSCs sheet wrapping around the MC/DPSCs or HA/TCP/DPSCs was implanted into the implant socket of four miniature pigs (the number was decided according to our previously reported success rate, in each miniature pig, left three sockets were MC group and right three sockets were HA/TCP group). In total, 12 bio-roots in MC group and 12 bio-roots in HA/TCP group were implanted in this study. The animals received 30 mg/kg penicillin by intramuscular injection to prevent infection. In order to evaluate the restorative potential of the bio-root and its efficacy to support an upper clinical crown, a crown restoration treatment was conducted after implantation for a period of 6 months. In brief, the gingiva at the implantation site was initially incised with a scalpel to expose the occlusal surface of the bio-root. Subsequently, the appropriate post-core for implantation was selected based on the diameter of the bio-root, and dental cement was utilized for cementation and photo-curing. Finally, an artificially fabricated porcelain crown was cemented in place.

Radiological evaluations and success rate analyses

Radiological evaluations, including computed tomography (CT) and micro-computed tomography (Micro CT, Inveon CT, Siemens AG, Munich, Germany) were performed on the regenerated bio-root after post-transplantation of 1 month, 3 months, 6 months, and 5 years respectively. Bio-root regeneration success rate was calculated according to the success criteria in our previous studies.⁵

Mechanical properties measurement

HA/TCP scaffold and MC scaffold were fabricated as cylindrical shapes of 8.5 mm in length and 4.0 mm in diameter, respectively. The elasticity modulus of these scaffolds was then evaluated through testing on a universal testing machine (SPL-10KNA, SHIMADZU, JAPAN). The pressure was conducted at a speed of 1 mm/min. The data were subjected to analysis through the plotting of stress-strain curves using Origin 2024 software. The modulus of elasticity was determined by calculating the slope of the linear range of variation.

Statistical analysis

All statistical calculations were performed using SPSS 13.0 statistical software. Student's *t*-test was conducted to compare the differences between two groups, one-way ANOVA was used when comparing three or more groups. If the data is non-normal distribution or unequal variances, Kruskal-Wallis and Mann-Whitney *U* tests were used to evaluate differences. *p* Value < 0.05 was considered statistically significant.

Results and discussion

Hierarchical structures of dentin, cementum, and alveolar bone

The dentin, cementum, and alveolar bone are the key hard tissues of tooth root. In order to find the structure differences between these tissues, we analyzed the hierarchical structures at the nanometer, micrometer, millimeter, and macroscopic levels.

The prepared human dentin slices were observed using optical microscopy, scanning electron microscopy (SEM), and transmission electron microscopy (TEM; Figure 1(a)). In dentin, the collagen fibers formed mineralized collagen fibrils, which comprised layers of plate-shaped crystals that spanned the cross-section of the fibril (Figure 1(b) and (c)). The collagen fibrils were then self-assembled into collagen fibril bundles ranging in thickness from less than a micrometer to several micrometers (Figure 1(d)). The

collagen fibril bundles then arranged in different patterns and formed dentinal tubules, intertubular dentin (ITD), and peritubular dentin (PTD; Figure 1(e)). It can be seen that the typical structure of ITD and PTD exists in every dentinal tubule. Randomly scattered holes were observed on the inner walls of the dentinal tubules. ITD was composed of abundant mineralized collagen and fibril bundles array in an interwoven form, while PTD lacked collagen (Figure 1(f) and (g)). At the millimeter level, the dentin contains the predentin, mantle dentin, and radicular dentin. The predentin adjacent to the pulp, was approximately 10–20 μm thick when stained with hematoxylin and eosin (H&E) under optical microscopy. The SEM images of the predentin showed a much looser collagen fibril net (Figure 1(h) and (h')). The unstained ground section and SEM images showed the presence of mantle dentin, which contained both ordered and disordered collagen fibrils. The ordered fibrils were parallel to the tubules, adjacent to their lumen, and surrounded by disordered collagen fibrils (Figure 1(i) and (i')). Optical and SEM images of radicular dentin displayed that the hyaline layer adjacent to the dentin was composed of disordered interlaced collagen fibers. The fibrous arrangement was denser than that of predentin and mantle dentin (Figure 1(j) and (j')).

The TEM and SEM micrographs showed similar hierarchical structures in dentin and cementum at the nanometer to micrometer levels (Figure 2(a)–(c)). TEM images revealed three types of cementum on a millimeter scale: acellular extrinsic fiber cementum (AEFC), cellular intrinsic fiber cementum (CIFC), and cellular mixed stratified cementum (CMSC; Figure 2(d) and (e)). It could be observed that AEFC contains collagen fibers bundles that belong to extrinsic fibers (EFs) connecting to the main fibers of the periodontal ligament. The EFs were arranged densely, almost perpendicular to the root surface, and were not simple straight fiber bundles but showed branching and anastomosing (Figure 2(d) and (d')). CIFC often contained EFs as well as intrinsic fibers (IFs), as shown in the TEM micrographs. Among them, EFs exhibit branching and anastomosing like what is seen in AEFC and are encircled by the IFs, which fill the space between the EFs. However, the diameter of extrinsic fibers was thicker than the extrinsic fibers in AEFC (Figure 2(e) and (e')). CMSC usually consisted of stratified CIFC and AEFC (Figure 2(f) and (f')). In SEM micrographs, there was an alternation of highly mineralized dark and faint lines that were considered to be resting or incremental lines since they were formed during intermittent AEFC formation's resting phases. The alternating lamellae are very similar to those in compact bone. All collagen fibrils run parallel in a given plane, and their direction rotates from one plane to another (Figure 2(g)–(g')).

The SEM micrographs showed similar hierarchical structures in the dentin, cementum, and alveolar bone at the nanometer to micrometer levels (Figure 3(a)–(c)). The

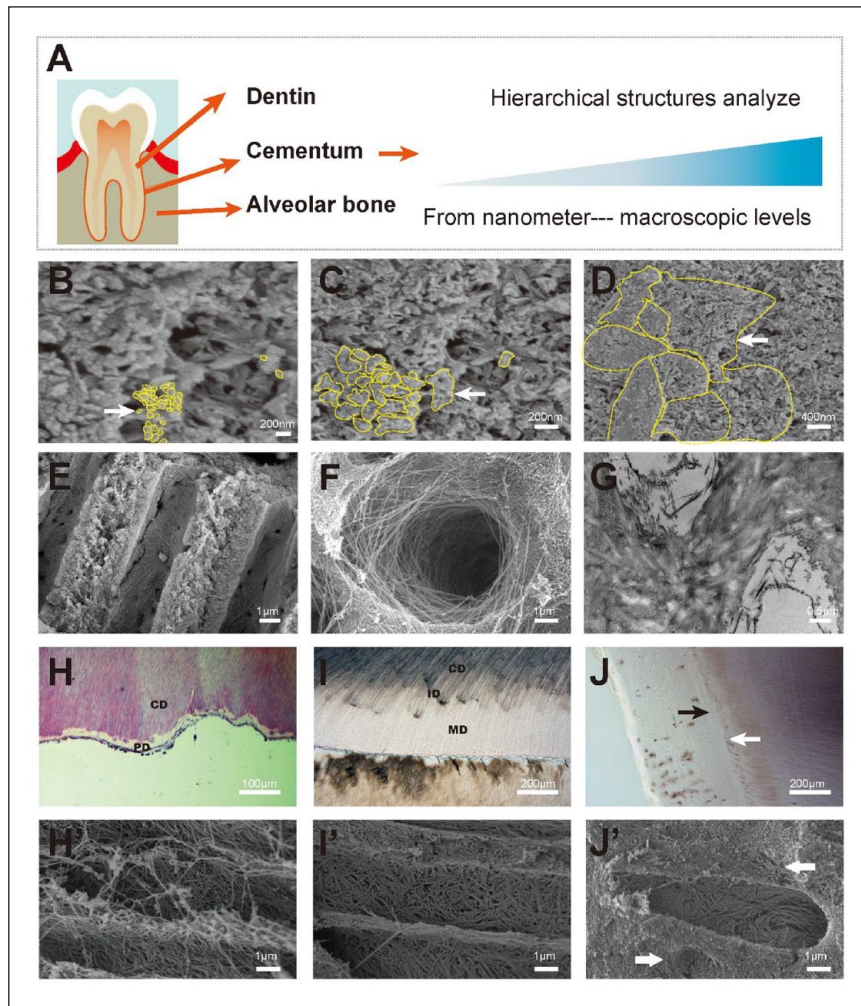


Figure 1. Characteristic structural levels of human dentin. (A) Schematic model of human dentin, cementum and alveolar bone hierarchical structure analysis. (B and C) The collagen fibers in dentin formed mineralized collagen fibrils. (D) The collagen fibrils were then self-assembled into collagen fibril bundles. The yellow lines and white arrows in b, c, and d showed the different cross-sectional dimensions of collagen fibril bundles in dentin ranging from nanometer to millimeter. (E, F, G) The collagen fibril bundles arrange in different patterns and formed dentinal tubules, intertubular dentin (ITD), and peritubular dentin (PTD). (H and H') The SEM images of the predentin showed a much looser collagen fibril net. (I and I') Mantle dentin was present in the unstained ground section and SEM images and contained ordered and disordered collagen fibrils. (J and J') Optical and SEM images of radicular dentin show the hyaline layer adjacent to the dentin was composed of disordered interlaced collagen fibers. The black and white arrows in J indicated the presence of hyaline layer and tomes granular layer. The white arrows in J' showed the presence of hyaline layer. The images in H, I, and J were derived from light microscopic observations conducted after the application of hematoxylin and eosin (H&E) staining. Scale bars represent 200 nm (B and C), 400 nm (D), 1 μ m (E, F, H', I', and J), 0.5 μ m (G), 100 μ m (H), and 200 μ m (I and J). CD: circumpulpal dentin; PD: predentin; MD: mantle dentin; and ID: interglobular dentin.

millimeter level structure of alveolar bone showed both an ordered and disordered array of fibril bundles. The disordered fibril bundles contained mineralized collagen fibrils that were abundant in the groundmass of the embedded osteocyte lacunae (Figure 3(d) and (d')). The major component of the ordered fibril bundles was also mineralized collagen fiber. The c-axes of the crystals were well aligned with the collagen fibril axis (in the interior or on the surface; Figure 3(e) and (e')). The alveolar bone contained both woven and parallel-fibered bone. Woven bone was composed of mineralized collagen fibril bundles with little

or no preferred orientation (Figure 3(f) and (f')). Parallel-fibril bone consisted mainly of unidirectionally ordered bundles of mineralized collagen fibrils. These bundles were separated by thin layers of disordered collagen fibril bundles. Lamellar bone was formed by a series of lamellae, each of which contained both ordered and disordered material in its embedded canaliculi. Each lamella contained differently oriented bundles of unidirectional arrays of mineralized fibrils and fanning arrays, and the spaces between these bundles were filled by the disordered material (Figure 3(g)). The canaliculi embedded in the

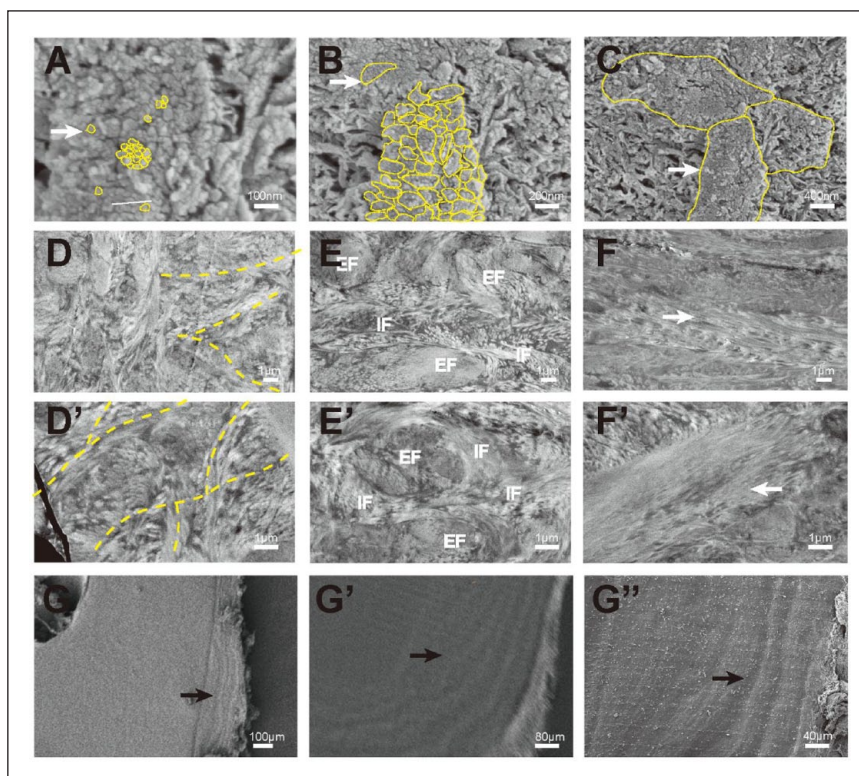


Figure 2. Characteristic structural levels of human cementum. (a, b, c) SEM micrograph of a mineralized collagen fibril to collagen fibril bundles in cementum. The yellow lines and corresponding white arrows indicated the diverse cross-sectional dimensions of collagen fibril bundles in cementum ranging from nanometer to millimeter. (d and d') TEM micrograph of acellular extrinsic fiber cementum. (e and e') TEM micrograph of cellular mixed stratified cementum. (f and f') TEM micrograph of cellular intrinsic fiber cementum. The white arrows indicated the location of fibers. (g, g', g'') SEM images of lamellar patterns (black arrows) during intermittent AEFC formation. Scale bars represent 100 nm (a), 200 nm (b), 400 nm (c), 1 μm (d, d'; e, e'; and f, f'), 100 μm (g), 80 μm (g'), and 40 μm (g'').

EF: extrinsic fibers; IF: intrinsic fibers.

disordered material were generally oriented perpendicular to the lamellar boundary plane. These results confirmed the hierarchical structures of alveolar bone (Figure 3(h)).

The difference of hierarchical structures in dentin, cementum, and alveolar bone

Hierarchical self-assembly is a ubiquitous phenomenon in life systems and is one of the most essential components of life.¹² Various natural biomaterials (structural proteins, nucleic acids, biofilms, and liposomes) are formed via hierarchical self-assembly.^{13–15} The hierarchical process of these molecules is a hot topic in multidisciplinary research.¹⁶ To date, the 12 hierarchical levels model for the mineral tissue has been detailedly outlined.⁸ As the biomineralization process is similar, we only detected the major levels from a nanometer-micrometer-millimeter-macroscopic scales in dentin, cementum, and alveolar bone instead of detecting all the 12 hierarchical levels. Our data showed that the collagen fibrils in dentin, cementum, and alveolar bone self-assembled into collagen fibril bundles. Collagen fibrils were assembled from type I collagen and hydroxyapatite

(HA, $\text{Ca}_{10}(\text{PO}_4)_6(\text{OH})_2$) nanocrystals, which was deposited along the collagen fibrils.¹⁷ The pattern was widely observed among human enamel, human long bones, zebrafish vertebrae, and collagen calcium phosphate mineralization synthetic materials.^{18–20} However, based on the arrangement of collagen fibril bundles, our data visually revealed differences in their hierarchical structures (Figure 4(a)). In dentin, the collagen fibril bundles formed dentinal tubules, intertubular dentin (ITD), and peritubular dentin (PTD). In cementum, the typical acellular extrinsic fiber cementum (AEFC), which contained collagen fiber bundles belonging to extrinsic fibers (EFs) that were connected to the main fibers of the periodontal ligament. The EFs were arranged densely, and appeared nearly perpendicular to the root surface. The millimeter-level structure of alveolar bone showed both an ordered and disordered array of fibril bundles. The disordered fibril bundles contained mineralized collagen fibrils, while the ordered bundles were separated from each other by thin layers of disordered collagen-fibril bundles. The typical hierarchical structure of the collagen fibril bundle arrangement model of dentin, cementum and alveolar bone were shown in Figure 4(b).

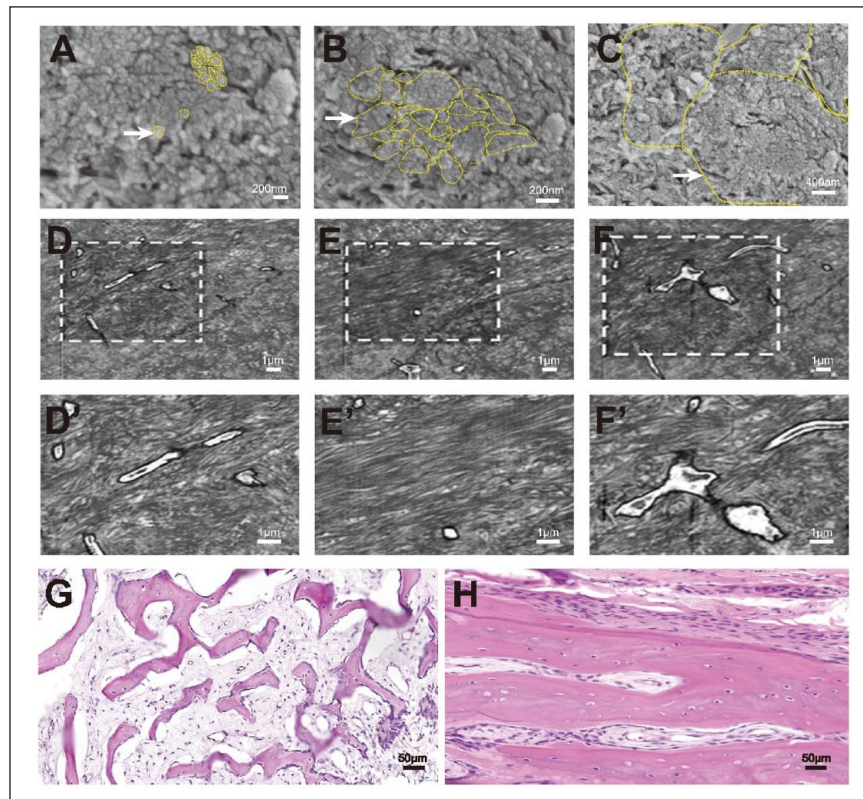


Figure 3. Characteristic structural levels of human alveolar bone. (a, b, c) SEM micrograph of a mineralized collagen fibril to collagen fibril bundles in alveolar bone. The yellow lines and corresponding white arrows indicated the various cross-sectional dimensions of collagen fibril bundles in alveolar bone ranging from nanometer to millimeter. (d and d') SEM micrograph showed the disordered fibril bundles also contained mineralized collagen fibrils that were abundant in the groundmass of the embedded osteocyte lacunae. (e and e') The major component of the ordered fibril bundles is mineralized collagen fiber. (f and f') Woven bone is composed of mineralized collagen fibril bundles with little or no preferred orientation. (g) Optical microscopy images of woven bone. (h) optical microscopy images of parallel fibered bone. Scale bars represent 200 nm (a and b), 400 nm (c), 1 μm (d, d'; e, e'; and f, f'), and 50 μm (g and h).

Differential expression of collagen genes in dentin, cementum, and alveolar bone

To further investigate the differentially expressed genes in the tooth tissues, we conducted RNA-SMART sequencing to compare gene expression levels in the dentin, cementum, and periodontal ligaments (Supplemental Figure S2). The specific gene expressions in dentin, by compared to cementum and periodontal ligament, were depicted. In addition, we observed differential expression levels of collagen genes in dentin, cementum, and alveolar bone, PCR array analysis was performed and the heatmaps were generated (Figure 5(a)–(c)). COL1A1 was identified as the dominant collagen gene in dentin, cementum, and alveolar bone. However, the expression levels of other collagen genes differed significantly among the three mineralized tissues. In particular, COL5A2, 1A2, and 20A1 were dominant in dentin, whereas COL28A1, 15A1, and 21A1 were prominent in cementum, and COL9A3, 1A1, and 4A4 were dominant in alveolar bone. The most significant

differentially expressed genes in these mineralized tissues were COL5A2, COL28A1, and COL9A3, respectively. Taken together, these results indicated that differences in the expression levels of collagen genes may be an important factor responsible for the structural differences between these mineralized tissues. Different developmental processes are crucial to the structural differences, which are attributed to factors such as variations in gene regulation, cell type, cell activity, and cell metabolism.²¹ The mineralization and hierarchical self-assembly processes occurred in the cell and extracellular matrix and were strictly controlled, which include collagen, HA, non-collagenous proteins and others. As the major difference is collagen fibril bundles arrangement, we first examined and compared the differential expression of collagen genes in dentin, cementum, and alveolar bone. We found that COL1A1 is the main collagen gene among dentin, cementum, and alveolar bone. But other collagen genes were expressed differently between the three mineralized tissue. In particular, dentin was dominated by COL5A2, 1A2, and

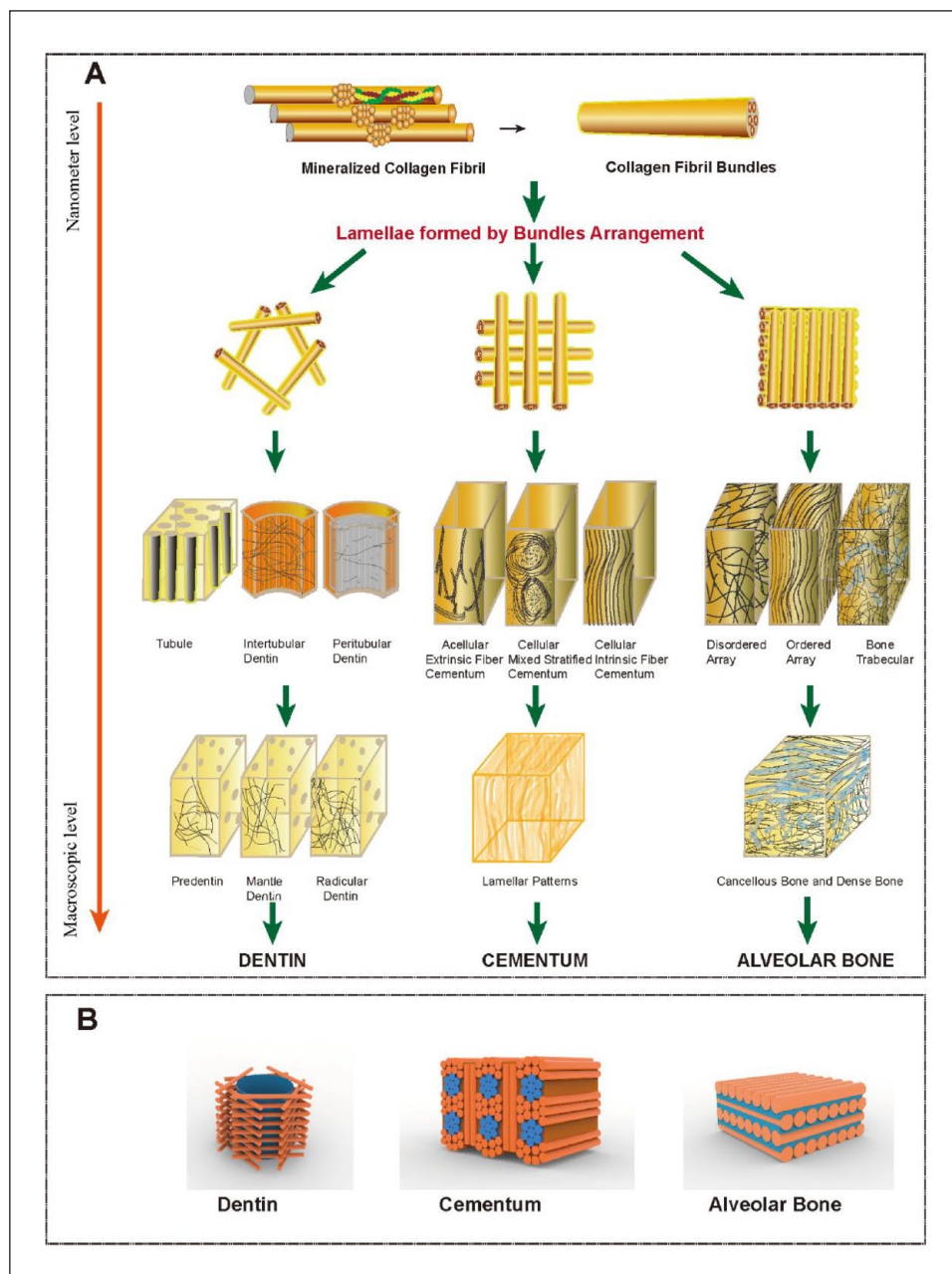


Figure 4. Characteristic differential structures of collagen fibril bundles in dentin, cementum, and alveolar bone. (a) The dentin, cementum, and alveolar bone have similar hierarchical structures from the collagen fibrils self-assembled into collagen fibril bundles. However, from the collagen fibril bundles arrangement, the differences between their hierarchical structures were manifested visually differently. In dentin, the collagen fibril bundles formed dentinal tubules, intertubular dentin (ITD), and peritubular dentin (PTD). In cementum, the typical acellular extrinsic fiber cementum (AEFC) containing collagen fiber bundles belonging to extrinsic fibers (EFs) connected to the main fibers of the periodontal ligament. The EFs were arranged densely, and appeared nearly perpendicular to the root surface. The millimeter-level structure of alveolar bone showed both an ordered and disordered array of fibril bundles. The disordered fibril bundles contained mineralized collagen fibrils, while the ordered bundles were separated from each other by thin layers of disordered collagen-fibril bundles. (b) Schematic model of collagen fibril bundle arrangement in dentin, cementum, and alveolar bone.

20A1, cementum was dominated by COL28A1, 15A1, and 21A1, and alveolar bone was dominated by COL9A3, 1A1, and 4A4. Previous studies have suggested that the directional and ordered growth of carbonated hydroxyapatite crystals is regulated by organic collagen, which is the

basic principle of the hierarchical self-assembly structure.²² Thus the different collagen fibril bundles arrangement may be due to the different collagen gene expression patterns in dentin, cementum, and alveolar bone, which need further be investigated.

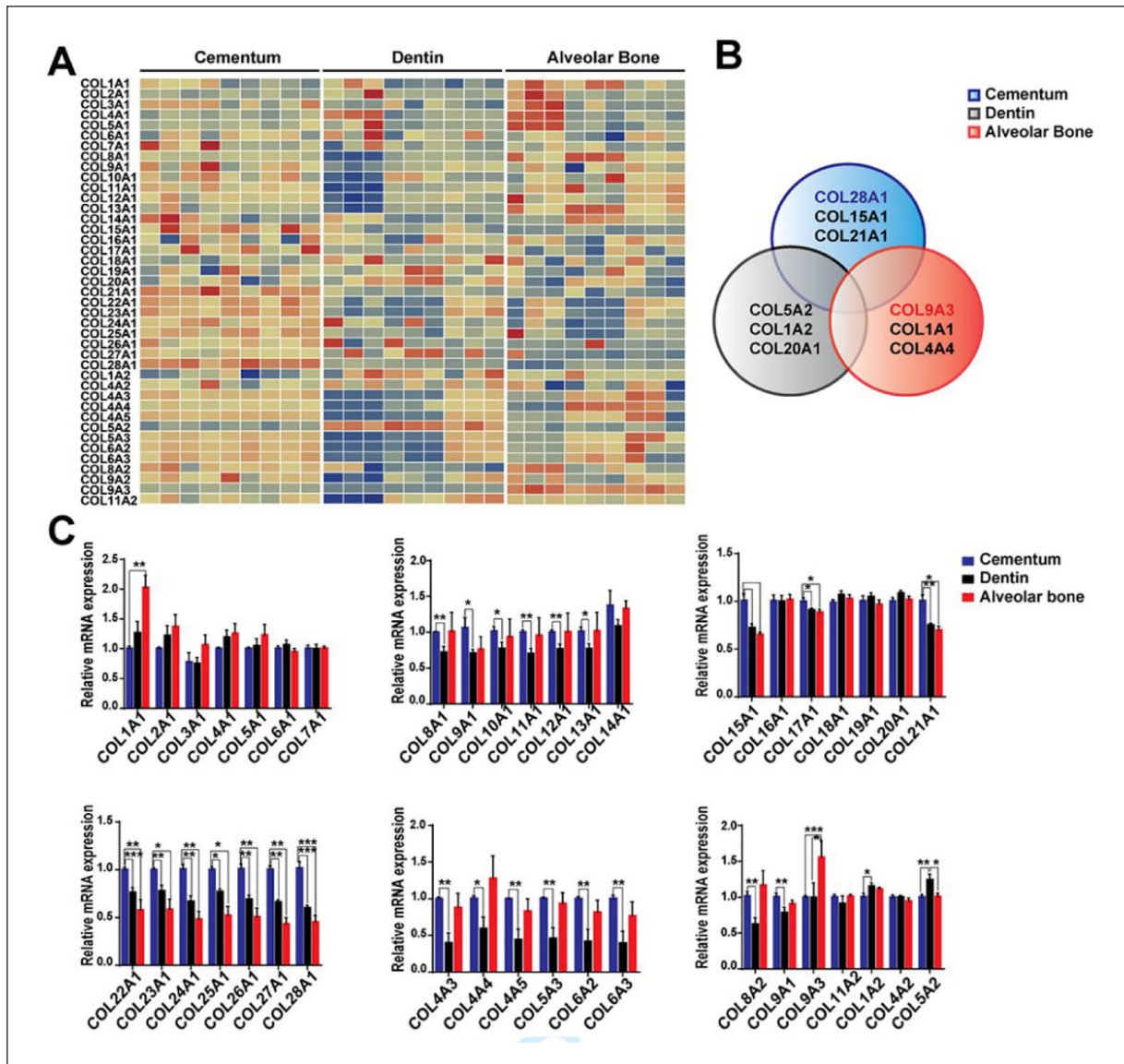


Figure 5. Differential expression of collagen genes in dentin, cementum, and alveolar bone. (a) Heat map of 44 differentially expressed collagen genes between dentin, cementum, and alveolar bone. Red and blue denote upregulated and downregulated genes, respectively. Further, the samples and genes are represented in rows and columns, respectively; $n=5$. (b) Venn diagram showing overlapping and differentially dominant collagen genes in dentin, cementum, and alveolar bone. (c) Quantitative real-time reverse transcriptase-PCR analysis of significant differentially expressed collagen genes in cementum, dentin, and alveolar bone samples. Gene expression was normalized to that of GAPDH. Data corresponding to three independent experiments are presented as mean \pm SD, one-way ANOVA was performed to determine statistical significance (* $p < 0.05$ and ** $p < 0.01$).

Developed MC scaffold and its effects on the proliferation and oste/odontogenesis of DPSCs *in vitro* and *in vivo*

Dentin, the main component of tooth roots, plays a central role in root regeneration. In our previous study using HA/TCP for bio-root regeneration, even though the tissue structure was similar to that of bone, we only observed 26% complete regeneration.⁵ HA/TCP is a classic artificial bone material that does not contain root structures or

components. However, it exhibits weak odontogenic induction and low load-bearing capacities for dental tissue regeneration. Thus, it is challenging to maintain its integrity during and after surgery.²³ Recently, hierarchical scaffolds that mimic the biomineralization process of mineral tissue have shown promising applications in regenerative medicine.^{9,24} By mimicking the natural biomineralization process via intra- or extra-fibrillar mineralization of collagen fibrils, tissue regeneration potential, such as the regeneration of bone or dentin, has been

considerably enhanced.^{25–28} The mineralization and hierarchical self-assembly processes occur in the cell and extracellular matrix, and are strictly controlled by collagen, HA, non-collagenous proteins. Although dentin and bone exhibit different structures and mechanical properties, the process of dentin formation is similar to that of other mineralized tissues,⁸ with self-assembled collagen fibrils providing a template for the specific localization of non-collagenous proteins and guiding further crystal growth.²⁹ Mimicking the initiation of biomineralization makes it difficult to regenerate bio-root with a specific dentin structure. Instead, considering the explicit differences between dentin and bone in the middle to the late stage of the hierarchical self-assembly process, we constructed an artificial scaffold, named “engineered pre-dentin,” by crosslinking bovine tendon-derived collagen I and HA, which showed a high-level similarity in hierarchical structure of dentin. This scaffold may be a promising strategy for bio-root regeneration. At first, we first investigated the hierarchical structure of the human tooth dentin and found that its collagen fibril bundles were arranged in different patterns and formed dentinal tubules, which was very different from the previously reported structure.⁸ SEM performed to analyze the structure of dentin showed that dentin was composed of mineralized collagen fibrils, which self-assembled into collagen fibril bundles (Figure 6(a)–(c)). Thus, collagen was used to successfully construct the MC by inducing the self-assembly of collagen in a dentin-like arrangement (Figure 6(d) and (e)). SEM also revealed that the characteristics of the MC were similar to those of natural dentin (Figure 6(f)). Further, we inoculated the MC scaffold with DPSCs followed by incubation in a mineralization medium. On days 7 and 14, qRT-PCR analysis showed significantly higher expression levels in MC group of ALP, COL-1, BSP, DSPP, ON, and OSX than those in the HA/TCP control group (Figure 6(g)). In addition, to evaluate the mechanical properties of scaffolds, we measured the elasticity modulus of HA/TCP and MC scaffolds (Supplemental Table S2). The results showed that elasticity modulus of HA/TCP and MC scaffolds were significantly lower than that of natural dentin (18.6 GPa).

To determine the role of MC and HA/TCP in DPSC odontogenic differentiation, the DPSCs were inoculated on scaffolds and transplanted subcutaneously into nude mice for 2 months. The results of hematoxylin and eosin (H&E) staining and Masson staining indicated a notably high proportion of newly mineralized tissues in the MC group compared to the HA/TCP group (Figure 7(a)–(g)). Additionally, the expression level of DSPP in the MC group was significantly higher than that in the HA/TCP group (Figure 7(h)–(n)). Furthermore, we compared several widely used materials, including polycaprolactone³⁰ and poly lactide-co- glycolic acid,^{31–34} and found that dentin-like tissue were significantly enhanced in MC group (Supplemental Figure S1 A–I). Previous studies have demonstrated that the mechanical properties of extracellular

matrix (ECM) influence the mesenchymal stem cell (MSC) differentiation capacity, especially in 3D culture environment.³⁵ The structure, composition and elasticity are the key points of ECM to regulate MSC behavior.³⁶ The area of diffusion matrix control differentiation of MSC. For example, in a small round matrix, MSCs undergo a notable differentiation into adipocytes, whereas the differentiation into osteoblasts is observed to increase in proportion to the matrix area.³⁷ In the present study, MC scaffold provided a 3D matrix mimicking the mineralized patterns of natural dentin to promote DPSC odontogenic differentiation. However, the elasticity modulus of MC scaffold was lower than natural dentin, indicating that the stiffness and supporting capacity of scaffold needs to be further improved to better simulate the *in vivo* environment and enhance differentiation of DPSC.

Dynamic observation of bio-root regeneration in nude mice

To compare the effects of MC and HA/TCP on bio-root regeneration, we first compared the effects of MC and HA/TCP on root regeneration in nude mice. H&E staining clearly showed PDLSCs sheets in the MC and HA/TCP groups after 1 week, and few DPSCs were found in the scaffolds (Figure 8(a)–(e)). From 2 weeks to 1 month, the PDLSCs sheets gradually regenerated in periodontal tissues and fused with surrounding tissues. Further, the DPSCs began to proliferate, and new tissues were regenerated in the inner scaffold. The number of regenerated tissues in the MC group was significantly higher than that in the HA/TCP group (Figure 8(f)–(o)). Three months later, the PDLSC sheet-regenerated tissues were completely fused with the surrounding tissues and could not be separated. In addition, the tissue regenerated inside the scaffold was mineralized and significantly increased. We also observed that the proportion of mineralized tissue in the MC group was significantly greater compared to the HA/TCP group (Figure 8(p)–(y)).

Bio-root functional regeneration in miniature pigs

To further clarify the effect of MC scaffolds on bio-root regeneration, MC and HA/TCP were used to construct bio-root scaffolds. The PDLSC sheet/DPSC sheet/DPSC/scaffold composite was constructed *in vitro* and transplanted into the mandibular area of miniature pigs. Six months later, crown restorations were performed for 5 years (Supplemental Figure S3A–D, Supplemental Figure S4). At third month, CT scans showed the formation of root-like structures with density similar to that of bone (Supplemental Figure S3E). After 5 years, three-dimensional CT images of the reconstructed natural tooth roots in the MC and HA/TCP groups showed a high-density

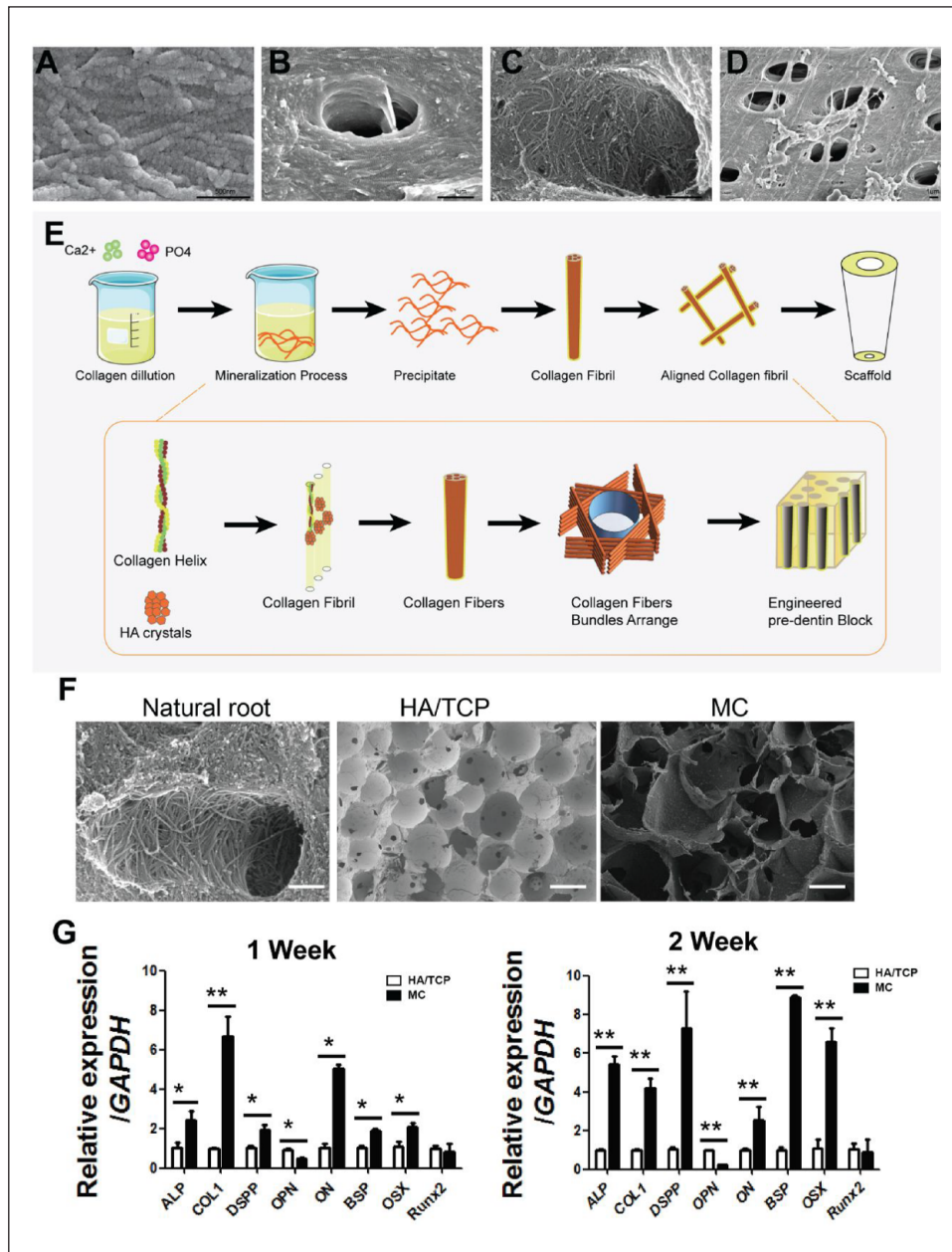


Figure 6. Dentin biomimetic MC promoted odontogenic DPSC differentiation *in vitro*. (a–d) Scanning electron microscopy (SEM) images of natural tooth dentin. (e) Scheme showing the process of MC construction as previously described (Zhao et al.¹⁰): collagen-mediated calcium phosphate mineralization process, precipitation of mineralized collagen microfibrils, preparation of MC fibrils, and alignment of obtained MC fibril array. (f) SEM images of natural tooth dentin, HA/TCP, and MC. (g) Real-time RT-PCR showing upregulated ALP, COL-1, BSP, DSPP, OPN, ON, Runx2, and OSX expression in DPSCs in the MC group relative to their expression levels in the HA/TCP group at 1 and 2 weeks. GAPDH was used as an internal control. Data based on three independent experiments are presented as mean \pm SD. Student's *t*-test was performed to determine statistical significance ($n = 5$). ** $p < 0.01$. Scale bars: 500 nm (a), 1 μ m (b, c, and d), and 500 nm (f).

root-shaped structure similar to that of natural teeth for both groups (Figure 9(a)–(c)). The regenerated root tissues in the MC and HA/TCP groups were surrounded by fibrous connective tissue and the fibers were similar to those in normal periodontal ligament (Figure 9(d)–(f)). The magnified images showed that the junction between mineralized tissue and soft ligament-like tissues are tightly bonded (Figure 9(g)–(i)). According to the success criteria for

bio-roots, 8 out of 12 complexes successfully regenerated bio-roots in the MC group, while two bio-roots were partially regenerated, and two bio-roots failed. In contrast, in the HA/TCP group, 4 of the 12 complexes successfully regenerated bio-roots, 4 bio-roots were partially regenerated, and 4 bio-roots failed (Figure 9(j)). The investigation of the microstructure of the regenerated bio-roots via SEM showed that the major component of the regenerated bio-roots in

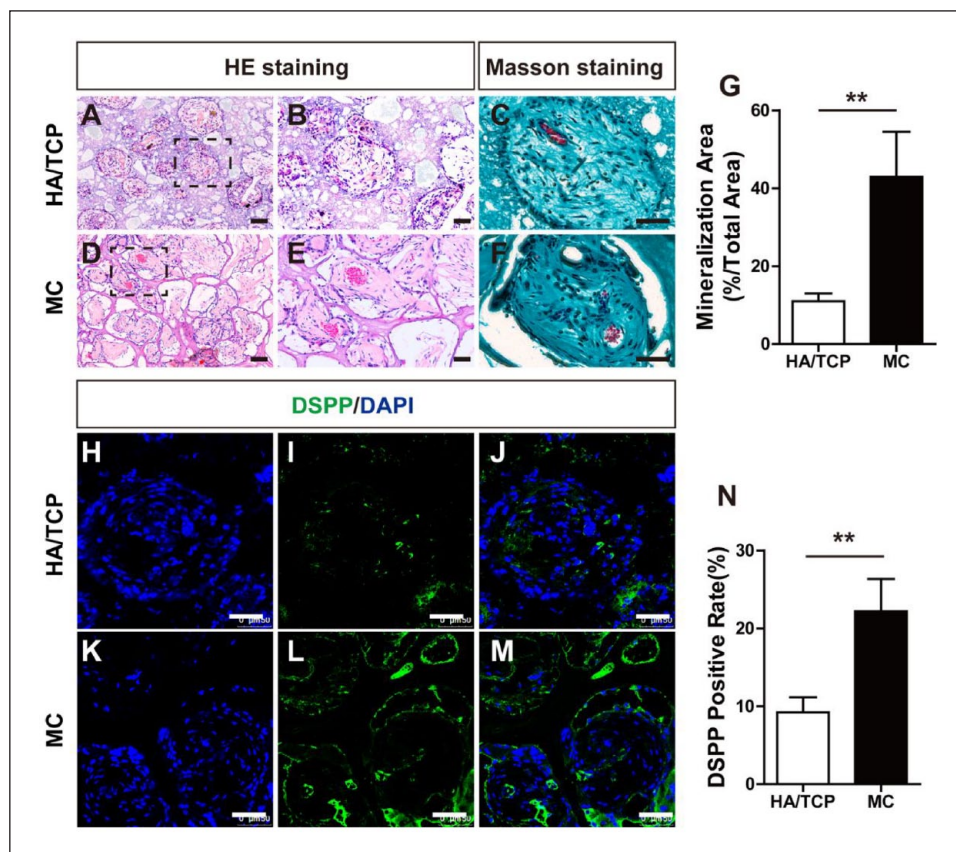


Figure 7. MC enhanced the odontogenesis of DPSCs *in vivo*. (a–f) Hematoxylin and Eosin staining and Masson's trichrome staining showing the formation of a more dental-like mineral tissue in the MC group than in the HA/TCP group 8 weeks after subcutaneous transplantation on the back of nude mice. (g) Qualitative measurements of mineralized tissue formation in different groups. (h–m) Immunofluorescence staining showing that MC enhanced DSPP expression in DPSCs to a greater extent than HA/TCP. Sections were counterstained with DAPI (blue). (n) Qualitative measurement of DSPP expression in different groups. Data corresponding to three independent experiments are presented as mean \pm SD. Student's *t*-test was performed to determine statistical significance ($n = 5$). Scale bars, 100 μ m.

* $p < 0.05$. ** $p < 0.01$. *** $p < 0.001$.

both the MC and HA/TCP groups was mineralized collagen fibers (Figure 9(k)–(p)). Notably, in the MC group, the structure of the regenerated bio-roots was composed of abundant mineralized collagen and fibril bundle arrays in an interwoven form. The typical structure of the dentinal tubules, that is, randomly scattered holes, surrounded by collagen fiber, was also observed; this is similar to the structure of natural dentin (Figure 9(m) and (p)). In the HA/TCP group, the regenerated bio-roots were composed mainly of unidirectionally ordered bundles of mineralized collagen fibrils that were separated from each other by thin layers of disordered collagen fibril bundles (Figure 9(l) and (o)). The MC scaffold promoted mineral tissue formation as well as the expression of DMP1, Col-I, and DSPP in DPSCs. In addition, it considerably promoted bio-root regeneration *in vivo*, and the regenerated bio-roots had a dentin-like collagen fibril bundle arrangement.

To verify the efficiency of bio-root to support a clinical crown, we conducted a upper crown restoration after

implantation (Supplemental Figure S4A–E). The results showed that bio-root sharing a dentin-like structure was robust enough to support an artificial clinical crown. However, the results of the mechanical examination demonstrated that the hardness and stiffness of the bio-root were markedly inferior to those of dentin. While satisfactory biocompatibility was observed, the ability of the bio-root to support long-term mastication remains to be evaluated over an extended period of time. Furthermore, the current limitations of the culture-induced nature of cell membrane sheets restrict the longevity of our constructed bio-root *in vitro*, which presents a challenge for its clinical translation. Future enhancements to the mechanical properties and optimization of the construction strategy will facilitate the clinical application of the bio-root. Our data showed the arrangement of collagen fibril bundles in MC would act as a template for dentin mineralization. The component of MC is type I collagen and HA, which have limited biological function. Combined the MC scaffold

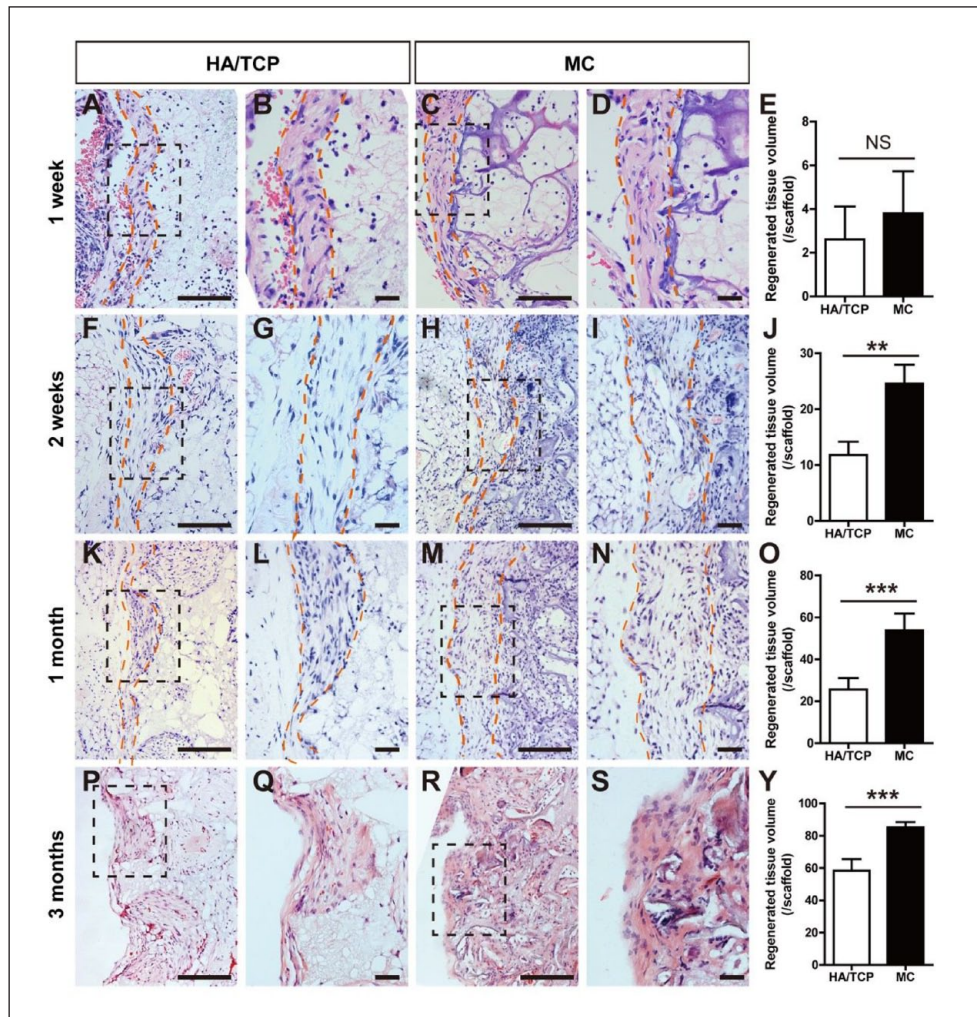


Figure 8. Dynamic observation of bio-root regeneration by MC and HA/TCP in nude mice. Root-shaped MC and HA/TCP were combined with DPSCs, coated with PDLSCs sheets, and subcutaneously transplanted into nude mice. Morphological analyses were then performed at 1 and 2 weeks and at 1 and 3 months after transplantation. Hematoxylin and Eosin staining clearly showed PDLSCs sheets in the MC and HA/TCP groups at 1 week, with few DPSCs in the scaffolds (a–e). At 2 weeks, the PDLSCs sheets gradually regenerated in periodontal tissues and fused with the surrounding tissues. Thus, DPSCs cells began to proliferate, and new tissues were regenerated in the inner scaffold. Significantly higher tissue regeneration was observed in the MC group than in the HA/TCP group (f–j). At 1-month, periodontal tissue and scaffold inner tissue regeneration increased in both the MC and HA/TCP groups, with the tissue regeneration significantly higher in the MC group than in the HA/TCP group (k–o). At 3 months, the PDLSC sheet-regenerated tissues were completely fused with the surrounding tissues and could not be separated, and the tissue regenerated inside the scaffold was mineralized and had increased significantly. Proportion of mineralized tissue significantly higher in the MC group than in the HA/TCP group (p–y). Data based on three independent experiments are presented as mean \pm SD. Student's *t*-test performed to determine statistical significance ($n=6$). Scale bars, 100 μ m.

** $p < 0.01$. *** $p < 0.001$.

with odontogenic differentiation agonist would significantly enhanced function of MC in bio-root regeneration, which need further investigation.

Conclusion

In conclusion, we demonstrated that the unique arrangement of collagen fibril bundles represents the major structural difference among dentin, cementum, and alveolar

bone. These structural differences may be attributed to variations in non-major collagen gene expression patterns. By mimicking the collagen fibril arrangement, the MC scaffold fabricated in this study could promote the odontogenesis of DPSCs as well as bio-root regeneration with structures and functions similar to those of natural tooth roots. MC scaffold could serve as a promising strategy for bio-root regeneration and tooth restoration by mimicking the natural structure of natural tooth.

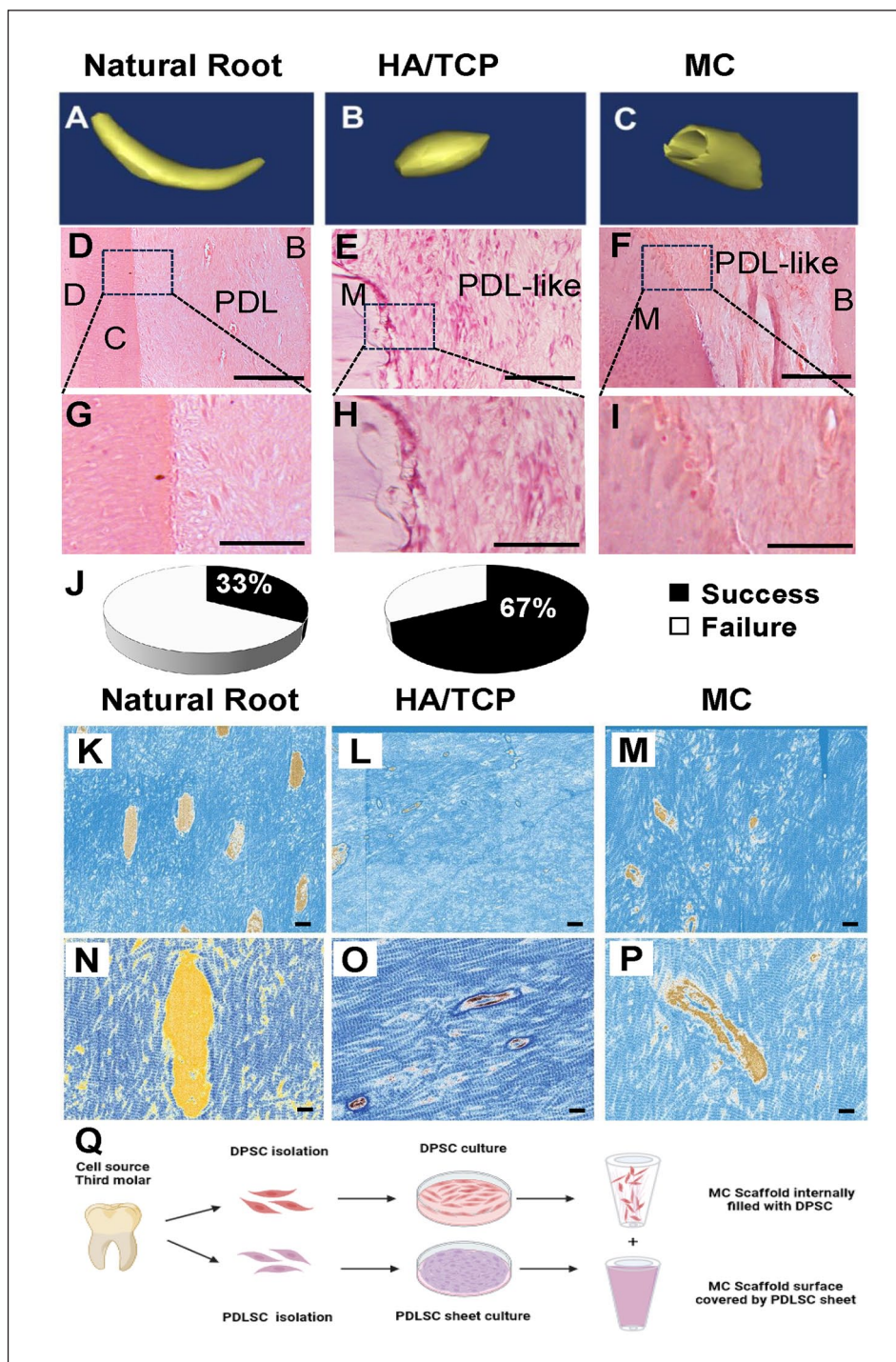


Figure 9. Histological and microstructure analyses of bio-roots after implantation. (a–c) Three-dimensional CT image reconstruction of natural tooth root and bio-root in the MC and HA/TCP groups, which was from *in vivo* implantation followed by a 5-year observation period. (d–f) Hematoxylin and Eosin staining of regenerated bio-root, showing periodontal ligament-like tissue and dentin-like tissue formation in the MC and HA/TCP groups relative to natural root. (g–i) The magnified images of the junction between soft and hard tissues. (j) Success rates of bio-roots in the MC and HA/TCP groups. Five years after implantation, the bio-root success rate with respect to complete regeneration in the MC group was 67% (8/12), while that in the HA/TCP group was 33% (4/12). SEM of the collagen fiber arrangement in natural root dentin (k and n), the HA/TCP group (l and o), and the MC group (m and p). The yellow part like randomly holes in H–K represented the structure of dentinal tubules. (q) Schematic diagram to display the combination of a scaffold with DPSC/PDLSC sheet. Created by BioRender. C: cementum; D: dentin; B: bone; M: Mineralized tissue. Scale bars, 50 μ m (d–f), 25 μ m (g–i), and 100 μ m (k–p).

Author's Note

Dongmei Cheng is also affiliated to Department of Oral Medicine, The Second Hospital of Hebei Medical University, Shijiazhuang, China

Authors contributions

Lei Hu contributed to design, data acquisition and analysis, interpretation, drafted, and critically revised the manuscript; Dongmei Cheng, Xin Yuan, Qiao Yi, Bin Zhao, Zhenhua Gao, Fulan Wei, Junji Xu, Zhipeng Fan, Yi Liu, Xiumei Wang, and Fuzhai Cui contributed to conception and design, critically revised the manuscript; Chunmei Zhang and Jinsong Wang contributed to acquisition and analysis, critically revised the manuscript; Songlin Wang contributed to conception, design, data analysis, interpretation and funding, drafted, and critically revised the manuscript.

Availability of data and materials

All the data to prove the conclusion are present in the paper and Supplementary materials, which will be available on any reasonable request from the authors.

Declaration of conflicting interests

The author(s) declared no potential conflicts of interest with respect to the research, authorship, and/or publication of this article.

Funding

The author(s) disclosed receipt of the following financial support for the research, authorship, and/or publication of this article: This work was supported by the Beijing Municipal Government grant (Beijing Laboratory of Oral Health, PXM2021-014226-000041); the Beijing Municipal Science and Technology Commission (Z181100001718208); the Beijing Municipal Education Commission (119207020201); the Innovation Research Team Project of Beijing Stomatological Hospital, Capital Medical University (CXTD202201); the Chinese Research Unit of Tooth Development and Regeneration, Academy of Medical Sciences (2019-12M-5-031); the National Natural Science Foundation of China (92049201, 82030031, 81991504, 92149301, L2224038, and 82001067); the Beijing Advanced Innovation Center for Big Data-based Precision Medicine (PXM2021_014226_000026); the Beijing Municipal Government (Beijing Scholar Program, PXM2020_014226_000005 and PXM2021_014226_000020); the Beijing Municipal Colleges and Universities High Level Talents Introduction and Cultivate Project-Beijing Great Wall Scholar Program (CIT&TCD 20180332); the National Key Research and development Program (2022YFA1104401); Scientific Research Common Program of Beijing Municipal Commission of Education (KM202110025009); and Beijing Municipal Natural Science Foundation (7232071).

Ethical approval

The animal study was approved by the Animal Care and Use Committee of Capital Medical University (AEEI-2015-080).

ORCID iD

Lei Hu  <https://orcid.org/0000-0002-4710-3707>

Supplemental material

Supplemental material for this article is available online.

References

- Oshima M and Tsuji T. Whole tooth regeneration as a future dental treatment. *Adv Exp Med Biol* 2015; 881: 255–269.
- Ikeda E, Morita R, Nakao K, et al. Fully functional bioengineered tooth replacement as an organ replacement therapy. *Proc Natl Acad Sci USA* 2009; 106: 13475–13480.
- Sonoyama W, Liu Y, Fang D, et al. Mesenchymal stem cell-mediated functional tooth regeneration in swine. *PLoS One* 2006; 1: e79.
- Wei F, Song T, Ding G, et al. Functional tooth restoration by allogeneic mesenchymal stem cell-based bio-root regeneration in swine. *Stem Cells Dev* 2013; 22: 1752–1762.
- Gao ZH, Hu L, Liu GL, et al. Bio-root and implant-based restoration as a tooth replacement alternative. *J Dent Res* 2016; 95: 642–649.
- Linde A and Goldberg M. Dentinogenesis. *Crit Rev Oral Biol Med* 1993; 4: 679–728.
- Caruso S, Bernardi S, Pasini M, et al. The process of mineralisation in the development of human tooth. *Eur J Paediatr Dent* 2016; 17: 322–326.
- Reznikov N, Bilton M, Lari L, et al. Fractal-like hierarchical organization of bone begins at the nanoscale. *Science* 2018; 360: eaao2189.
- Yu L and Wei M. Biomineralization of collagen-based materials for hard tissue repair. *Int J Mol Sci* 2021; 22: 20210119.
- Zhao Y, Zheng J, Xiong Y, et al. Hierarchically engineered artificial lamellar bone with high strength and toughness. *Small Struct* 2023; 4: 2200256.
- Yu M, Luo D, Qiao J, et al. A hierarchical bilayer architecture for complex tissue regeneration. *Bioact Mater* 2022; 10: 93–106.
- Liu Y, Luo D and Wang T. Hierarchical structures of bone and bioinspired bone tissue engineering. *Small* 2016; 12: 4611–4632.
- Lazcano A. Prebiotic evolution and self-assembly of nucleic acids. *ACS Nano* 2018; 12: 9643–9647.
- Lim SWZ, Wong YS, Czarny B, et al. Microfluidic-directed self-assembly of liposomes: role of interdigitation. *J Colloid Interface Sci* 2020; 578: 47–57.
- Onur T, Yuca E, Olmez TT, et al. Self-assembly of bacterial amyloid protein nanomaterials on solid surfaces. *J Colloid Interface Sci* 2018; 520: 145–154.
- Yamamoto T, Hasegawa T, Hongo H, et al. Alternating lamellar structure in human cellular cementum and rat compact bone: its structure and formation. *J Oral Biosci* 2019; 61: 105–114.
- Micheletti C, Hurley A, Gourrier A, et al. Bone mineral organization at the mesoscale: a review of mineral ellipsoids in bone and at bone interfaces. *Acta Biomater* 2022; 142: 1–13.
- Chang Z, Chen PY, Chuang YJ, et al. Zebrafish as a model to study bone maturation: nanoscale structural and mechanical characterization of age-related changes in the zebrafish vertebral column. *J Mech Behav Biomed Mater* 2018; 84: 54–63.
- Cui FZ and Ge J. New observations of the hierarchical structure of human enamel, from nanoscale to microscale. *J Tissue Eng Regen Med* 2007; 1: 185–191.

20. de Melo Pereira D and Habibovic P. Biomaterialization-inspired material design for bone regeneration. *Adv Healthc Mater* 2018; 7: e1800700.
21. Yamamoto T, Hasegawa T, Yamamoto T, et al. Histology of human cementum: its structure, function, and development. *Jpn Dent Sci Rev* 2016; 52: 63–74.
22. Costa PF, Vaquette C, Zhang Q, et al. Advanced tissue engineering scaffold design for regeneration of the complex hierarchical periodontal structure. *J Clin Periodontol* 2014; 41: 283–294.
23. Balçık C, Tokdemir T, Senköylü A, et al. Early weight bearing of porous HA/TCP (60/40) ceramics in vivo: a longitudinal study in a segmental bone defect model of rabbit. *Acta Biomater* 2007; 3: 985–996.
24. Puetzer JL, Ma T, Sallent I, et al. Driving hierarchical collagen fiber formation for functional tendon, ligament, and meniscus replacement. *Biomaterials* 2021; 269: 120527.
25. Padovano JD, Ravindran S, Snee PT, et al. DMP1-derived peptides promote remineralization of human dentin. *J Dent Res* 2015; 94: 608–614.
26. Jin SS, He DQ, Luo D, et al. A biomimetic hierarchical nanointerface orchestrates macrophage polarization and mesenchymal stem cell recruitment to promote endogenous bone regeneration. *ACS Nano* 2019; 13: 6581–6595.
27. Thirivikraman G, Athirasala A, Gordon R, et al. Rapid fabrication of vascularized and innervated cell-laden bone models with biomimetic intrafibrillar collagen mineralization. *Nat Commun* 2019; 10: 3520.
28. Zhao Y and Tang R. Improvement of organisms by biomimetic mineralization: a material incorporation strategy for biological modification. *Acta Biomater* 2021; 120: 57–80.
29. Moradian-Oldak J and George A. Biomaterialization of enamel and dentin mediated by matrix proteins. *J Dent Res* 2021; 100: 1020–1029.
30. D'Antò V, Raucci MG, Guarino V, et al. Behaviour of human mesenchymal stem cells on chemically synthesized HA-PCL scaffolds for hard tissue regeneration. *J Tissue Eng Regen Med* 2016; 10: E147–E154.
31. Raddall G, Mello I and Leung BM. Biomaterials and scaffold design strategies for regenerative endodontic therapy. *Front Bioeng Biotechnol* 2019; 7: 317.
32. He L, Zhou J, Chen M, et al. Parenchymal and stromal tissue regeneration of tooth organ by pivotal signals reinstated in decellularized matrix. *Nat Mater* 2019; 18: 627–637.
33. Liang Y, Luan X and Liu X. Recent advances in periodontal regeneration: a biomaterial perspective. *Bioact Mater* 2020; 5: 297–308.
34. Jazayeri HE, Lee SM, Kuhn L, et al. Polymeric scaffolds for dental pulp tissue engineering: a review. *Dent Mater* 2020; 36: e47–e58.
35. Saraswathibhatla A, Indana D and Chaudhuri O. Cell-extracellular matrix mechanotransduction in 3D. *Nat Rev Mol Cell Biol* 2023; 24: 495–516.
36. Price RL, Ellison K, Haberstroh KM, et al. Nanometer surface roughness increases select osteoblast adhesion on carbon nanofiber compacts. *J Biomed Mater Res A* 2004; 70: 129–138.
37. McBeath R, Pirone DM, Nelson CM, et al. Cell shape, cytoskeletal tension, and RhoA regulate stem cell lineage commitment. *Dev Cell* 2004; 6: 483–495.